Analyst

Cite this: *Analyst*, 2011, **136**, 2367

www.rsc.org/analyst

**PAPER**

# $Pb^{2+}$ induced DNA conformational switch from hairpin to G-quadruplex: electrochemical detection of $Pb^{2+}$†

**Zhenzhen Lin, Yue Chen, Xiaohong Li* and Weihai Fang***

***Received 28th January 2011, Accepted 17th March 2011***
**DOI: 10.1039/c1an15080d**



Conformational switch from hairpin DNA to G-quadruplex induced by $Pb^{2+}$ is studied by electrochemical impedance spectroscopy (EIS) in the presence of $[Fe(CN)_6]^{3-/4-}$ as the redox probe. In the presence of $Pb^{2+}$, the G-rich hairpin DNA opens the stem-loop and forms G-quadruplex structure, which gives rise to a sharp increase in the charge-transfer resistance ($R_{CT}$) of the film reflected by the EIS. This structural change is also confirmed by circular dichroism (CD) measurements and UV-Vis spectroscopic analysis and calculated by density functional theory (DFT). On the basis of this, we develop a label-free electrochemical DNA biosensor for $Pb^{2+}$ detection. With increasing concentrations of $Pb^{2+}$, the differences in the charge-transfer resistance $R_{CT}$ before and after the $Pb^{2+}$ incubation is linearly dependent on the logarithm of $Pb^{2+}$ concentration within a range from 50 μM to 0.5 nM. The biosensor also exhibits good selectivity for $Pb^{2+}$ over other metal ions. This is a simple and label-free electrochemical method for $Pb^{2+}$ detection making use of the G-quadruplex.

## Introduction

Lead ions, which are one of the most toxic contaminants in aquatic ecosystems, pose a severe risk for human health and the environment.[1] Therefore, sensitive and on-site tracking of $Pb^{2+}$ in aqueous media is of great importance in environmental and food monitoring, as well as clinical toxicology. Recent years have witnessed great progress in the development of optical sensors based on DNA,[2–21] and most of them are focused on the lead-dependent 8–17 DNAzyme,[2–16,19–21] which can be combined with fluorophore/quencher pairs,[2–10] nanoparticles[11–15] and other DNAzymes.[16] For example, Lu *et al.* constructed a series of $Pb^{2+}$ optical sensors exploiting a fluorophore-quenching mechanism[3–10] and the deaggregation of Au nanoparticles in response to the $Pb^{2+}$–DNAzyme system.[11–15] Willner *et al.* made use of the horseradish peroxidase-mimicking DNAzyme activated by the interaction between $Pb^{2+}$ and 8–17DNAzyme.[16] Compared to these optical assays, only a few electrochemical DNA sensors for $Pb^{2+}$ detection were designed, which are still based on the $Pb^{2+}$–DNAzyme.[22–24] Although these optical and electrochemical assays are versatile, DNAzyme is vulnerable to *in vivo* detection or complex systems when it comes to practical use. So, it is necessary to develop a new electrochemical assay for avoiding the application of classic $Pb^{2+}$–DNAzyme as a sensing element.

Recently, some of DNA sensors for $Pb^{2+}$ detection have been based on $Pb^{2+}$ induced G-quadruplex formation upon the DNA sequences reacting with $Pb^{2+}$.[25–27] For example, Dong *et al.* developed a novel $Pb^{2+}$ sensor with a G-quadruplex DNAzyme by colorimetry and chemiluminescence (CL).[17] Chang *et al.* reported thrombin-binding aptamer (G-rich DNA) for $Pb^{2+}$ detection by fluorescence resonance energy transfer between a fluorophore and a quencher at the termini of each DNA probe.[18] Based on the results, the conclusion could be made that $Pb^{2+}$ can sensitively and selectively react with G-rich single-stranded DNA to form a G-quadruplex. Then what would happen when $Pb^{2+}$ reacts with unlabeled G-rich hairpin DNA? To the best of our knowledge, no electrochemical assay based on unlabeled G-rich hairpin DNA for $Pb^{2+}$ detection has been reported.

In this paper, we adopted a G-rich hairpin DNA sequence to investigate the $Pb^{2+}$ induced DNA conformational switch from hairpin to G-quadruplex by electrochemical impedance spectroscopy (EIS), and an obvious increase in $R_{CT}$ was observed. To further confirm this phenomenon, we adopted circular dichroism (CD) measurements and UV-Vis spectroscopic analysis to investigate this structure change and the results were in agreement with our speculation. And density functional theory (DFT) was employed to study the structures of hairpin DNA, G-quadruplex and the G-quadruplex–$Pb^{2+}$ complex. Results indicate that this switch is an exothermic process and irreversible. Taking advantage of the charge-transfer resistance ($R_{CT}$) change ($\Delta R_{CT}$), $Pb^{2+}$ can be detected at the concentration as low as 0.5 nM. Meanwhile, the sensor maintained highly selectivity over other non-specific metal ions. Based on these results, a simple, low-cost and label-free electrochemical biosensor for $Pb^{2+}$ was constructed, which holds great potential for $Pb^{2+}$ practical detection. In addition, the electrochemical approach based on

*Department of Chemistry, Beijing Normal University, Beijing, 100875. E-mail: lxhxiao@bnu.edu.cn; Fangwh@bnu.edu.cn; Tel: +086-01-58802741*

† Electronic supplementary information (ESI) available. See DOI: 10.1039/c1an15080d

the conformational switch can be further extended to other DNA-based systems to detect and quantify wider ranges of analytes.

## Experimental

### 1 Oligonucleotides and chemicals

Three DNA sequences (the underlined are complementary pairs) were synthesized by standard solid-phase techniques using a fully automated DNA synthesizer in Shanghai (Shanghai Sangon Biological Engineering Technology & Service Co.Ltd):

DNA(1): 5′-HO-$(CH_2)_6$-SS-$(CH_2)_6$-TTTTT-CCAAC-GGTTGG TGT-GGTTGG-3′

DNA(2): 5′-TTTTT-CCAAC-GGTTGG-TGT-GGTTGG-3′

The working gold electrodes, 99.99% (w/w) polycrystalline with a diameter of 1 mm were purchased from Aida Instrument Inc in Tianjin and cleaned prior to use. Tris (Tris-(hydroxymethyl)aminomethane), $NaClO_4$, $K_3[Fe(CN)_6]$, $K_4[Fe(CN)_6]$, $Pb(ClO_4)_2 \cdot 3H_2O$, $KClO_4$, $Zn(ClO_4)_2 \cdot 6H_2O$, $Ni(ClO_4)_2 \cdot 6H_2O$, $Co(ClO_4)_2 \cdot 6H_2O$, $Cd(ClO_4)_2 \cdot xH_2O$, $Cu(ClO_4)_2 \cdot 6H_2O$, $Mn(ClO_4)_2 \cdot 6H_2O$, $Al(ClO_4)_3 \cdot 9H_2O$, $LiClO_4$ and 6-mercaptohexanol were purchased from Aldrich and used without further purification. $Mg(ClO_4)_2$ was purchased from Fluka and used as received. Deionized water (18.2 MΩ cm resistivity) from a Millipore Milli-Q system was used through this work. The Tris buffer was adjusted to pH 7.4 with $HClO_4$. An Ag/AgCl reference electrode was added to the cell through a miniature salt bridge (agar plus $KNO_3$) to avoid any contamination due to $Cl^-$ from the reference electrode.

### 2 Monolayer preparation

The freshly cleaned gold electrodes (1.0 mm diameter) were incubated in a solution of 10 μM disulfide-modified hairpin-structured strand in 20 mM Tris-$ClO_4$ buffer (pH = 7.4) for 5 days. Then the electrodes were washed with the buffer solution and subsequently incubated in 1 mM 6-mercaptohexanol for 1 day. The electrodes were then washed with Tris-$ClO_4$ buffer and mounted into an electrochemical cell. After rinsing with the buffer, the electrodes were incubated for 1 day in a solution of $PbClO_4$ in 20 mM Tris-$ClO_4$ buffer (pH = 7.4). The EIS of the films were recorded.

### 3 Electrochemical measurements

A conventional three-electrode system was used, and all the measurements were carried out at room temperature in an enclosed and grounded Faraday cage. The reference electrode was constructed by sealing an Ag/AgCl wire into a glass tube with a solution of saturated KCl that was capped with a Vycor tip. The counter electrode was a platinum wire. Impedance spectra were measured using a potentiostat frequency analyzer (EG&G 2273). The ac voltage amplitude was 5 mV, and the voltage frequencies used for EIS measurements ranged from 100 kHz to 100 mHz. The applied potential was 250 mV *vs.* Ag/AgCl (formal potential of the redox probe $[Fe(CN)_6]^{3-/4-}$ in the buffer solution). All measurements were repeated for a minimum of five times with separate electrodes to obtain statistically meaningful results.

### 4 CD and UV-Vis spectroscopic analysis

A JASCO J-810 spectropolarimeter was utilized to collect the CD spectra of hairpin DNA(2) (2 μM) in the Tris-$ClO_4$ buffer (pH = 7.4) containing $Pb^{2+}/K^+$ or not at room temperature. The optical chamber is of 1 cm path length, 1.5 mL volume. Two scans (200 nm $min^{-1}$) from 350 to 225 nm at 0.5 nm intervals were accumulated and averaged. The background of the buffer solution was subtracted from the CD data.

The UV-Vis spectroscopic investigation of hairpin DNA(2) (2 μM) in the Tris-$ClO_4$ buffer (pH = 7.4) containing $Pb^{2+}$ or not was performed at room temperature. The absorption spectra of the reaction mixture were recorded with a Cazy 50 Scan UV-Vis Spectrophotometer in the wavelength range from 400 to 200 nm and a scan rate of 600 nm $min^{-1}$.

### 5 Computational detail

The hairpin DNA(1) chain has 20 nuclei acid units except the five 'T' bases as linker. All the phosphate moieties are replaced by phosphate ester. Then the whole molecule has 726 atoms. Density functional CAM-B3LYP[28] implemented in Gaussian 09 program package[29] was employed for optimization of the structures with mixed basis sets, where 3-21G* was used for C, N, O and H atoms and 6-31G* for P atoms and LANL2DZ for Pb atom.

## Results and discussion

### 1 $Pb^{2+}$ induced DNA conformational switch from hairpin to G-quadruplex

The hairpin DNA films were prepared by incubating freshly cleaned gold electrodes in solutions of 10 μM 25-mer DNA strand (1), followed by backfilling potential pinholes and defects by soaking the film in 1 mM 6-mercaptohexanol in 20 mM Tris-$ClO_4$. This procedure prevents the molecules from laying flat on the surface and aligns the immobilized DNA hairpins in an upright orientation.[30] Then the modified electrodes were incubated in 50 μM $PbClO_4$ solution. In the presence of $Pb^{2+}$, hairpin DNA opened the stem-loop structure and formed the $Pb^{2+}$ stabilized G-quadruplex as shown in Fig. 1. EIS was applied to track this process and the representative Nyquist plots for the films are shown in Fig. 2. The impedance spectra were analyzed with the help of a modified Randles' equivalent circuit, relating specific properties to resistive and capacitive components (inset of Fig. 2). The fitting results for the films are listed in Table 1.

The solution resistance, $R_s$, is the resistance between the reference electrode and the films of hairpin DNA on the gold electrodes. For each measurement, the position of the two electrodes is kept the same. All measurements were carried out under identical conditions of electrolyte concentration (20 mM Tris-$ClO_4$) and at room temperature to minimize variations in $R_s$, which ranged from 5.0 to 5.3 $\Omega \cdot cm^2$.

$C_{monolayer}$ accounts for the capacitance of the DNA films on the gold electrodes. In the presence of $Pb^{2+}$, the film capacitance $C_{monolayer}$ increased significantly from 7.5(0.6) to 9.7(0.2) $\mu F \cdot cm^{-2}$. The results could be rationalized that the structural switch from hairpin DNA to the more condensed G-quadruplex films result in a decrease in the film thickness.[31]

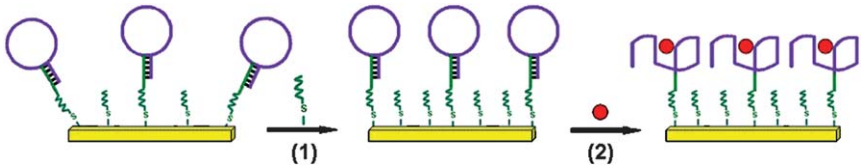


**Fig. 1** Schematic view of DNA conformational switch from hairpin to G-quadruplex induced by $Pb^{2+}$: (1) 6-mercaptohexanol is applied to occupy the possible pinholes on the electrode modified with thiolated hairpin DNA, and force the immobilized DNA to align reproducibly in an orientation extending away from the electrode surface; (2) in the presence of $Pb^{2+}$, hairpin DNA opens the stem-loop structure and forms the G-quadruplex.

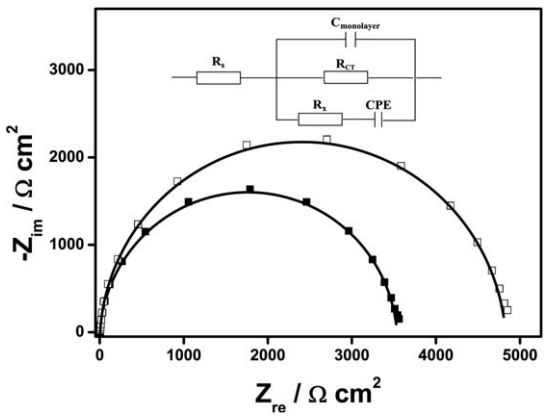


**Fig. 2** Representative Nyquist plots ($-Z_{im}$ *vs.* $Z_{re}$) for films of 25-mer hairpin DNA(1) before (■) and after incubating with 50 μM $Pb(ClO_4)_2$ solution (□). Measured data are shown as symbols with calculated fit to the equivalent circuit as solid lines. Inset: the measured data are fit to the equivalent circuit: $R_s$, solution resistance; $C_{monolayer}$, capacitance of the DNA monolayer film; $R_{CT}$, charge-transfer resistance of DNA monolayer film; $R_x$ and CPE, resistance and non-linear capacitor accounting for 6-mercaptohexanol film.

The combination of $R_x$ and the constant phase element (CPE) accounts for the behavior of the 6-mercaptohexanol-diluted films on the electrode surfaces. CPE acts as a non-linear capacitor accounting for the inhomogeneity of the films on the electrode surface with the exponential modifier $n = 0.8$.[32] Diffusion of the redox probe from the solution to the DNA film is not important in this system, as is apparent from the absence of any Warburg impedance as shown in Fig. 2.

The charge-transfer resistance, $R_{CT}$, is the result of the resistance to charge transfer from the solution-based redox probe $[Fe(CN)_6]^{3-/4-}$ to the electrode surface. In the presence of $Pb^{2+}$, $R_{CT}$ increased from 3340(146) $\Omega \cdot cm^2$ to 4877(137) $\Omega \cdot cm^2$ and the $R_{CT}$ difference ($\Delta R_{CT}$) is 1537(51) $\Omega \cdot cm^2$. This could be viewed as the result of the $Pb^{2+}$ induced DNA conformational switch from hairpin to G-quadruplex. Here, there are two functions of $Pb^{2+}$ in this system: one is its capability to open the stem-loop structure to form G-quadruplex, which produced larger surface negative charge density and resulted in the increased $R_{CT}$;[31] the other is its electrostatic interaction with the negative charges of the DNA backbone and resulted in the decreased $R_{CT}$.[33] In this case, electrostatic interaction is not dominant.

Next, the conformational switch was further analyzed by CD and UV-Vis spectroscopy. CD spectra for 2 μM hairpin DNA(2) in the absence and in the presence of 5 mM, 0.5 mM and 50 μM $Pb^{2+}$ were shown in Fig. 3A. In the absence of $Pb^{2+}$, CD spectrum was of relatively low amplitude due to hairpin oligonucleotides possessing a little chiral structure. When incubated in 0.5 mM and 50 μM $Pb^{2+}$, the spectra exhibited a long wavelength maximum near 312 nm, which is consistent with $Pb^{2+}$-stabilized antiparallel quadruplex structures.[25–27] In the presence of 5 mM $Pb^{2+}$, no obvious absorption peaks appeared. We attribute this phenomenon to the formation of lead hydroxide at pH 7.4 which may turn the solution into a suspension. As for UV-Vis spectroscopy for the 50 μM $Pb^{2+}$ + DNA system shown in Fig. 3B, compared to only hairpin DNA solution, the peak at 260 nm did not shift, but an obvious increase in intensity was observed. This indicated the unwinding of the base pairs in the stem-loop allowing more bases exposed. Based on the two experiments, we believed that the conformational switch as illustrated in Fig. 1 happened indeed.

Finally, electrostatic interaction between hairpin DNA and $Pb^{2+}$ was also explored. Firstly, G-rich hairpin DNA(1) films were incubated at higher concentrations of $Pb^{2+}$, such as 5 and 0.5 mM. In the case of 5 mM $Pb^{2+}$, electrostatic interaction was so strong that a sharp decrease in $R_{CT}$ was observed as shown in Fig. 4A. When the concentration decreased to 0.5 mM, it presented almost no change in $R_{CT}$ as shown in Fig. 4B, which was supposed to be a combination result of electrostatic interaction and conformational switch. Based on the results above, we can conclude that electrostatic interaction existed when the $Pb^{2+}$ concentration was higher.

In order to further confirm the specific interaction between DNA(1) and $Pb^{2+}$, an unspecific DNA(3) was chosen to react

**Table 1** Equivalent circuit element values for hairpin DNA films in absence and presence of 50 μM $Pb^{2+}$ [a]

| | Equivalent circuit elements | | | | | | |
|---|---|---|---|---|---|---|---|
| | $R_s/\Omega \cdot cm^2$ | $C_{monolayer}/\mu F \cdot cm^{-2}$ | $R_{CT}/\Omega \cdot cm^2$ | $R_x/\Omega \cdot cm^2$ | CPE/$\mu F \cdot cm^{-2}$ | $n$ | $\Delta R_{CT}/\Omega \cdot cm^2$ |
| Hairpin DNA | 5.1(0.2) | 7.5(0.6) | 3340(146) | 4.0(0.6) | 11.3(1.3) | 0.8(0.01) | — |
| Hairpin DNA + $Pb^{2+}$ | 5.2(0.5) | 9.7(0.2) | 4877(137) | 24.7(6.1) | 12.0(0.9) | 0.8(0.07) | 1537(51) |

[a] The values in parentheses represent the standard deviations from at least 5 electrode measurements.

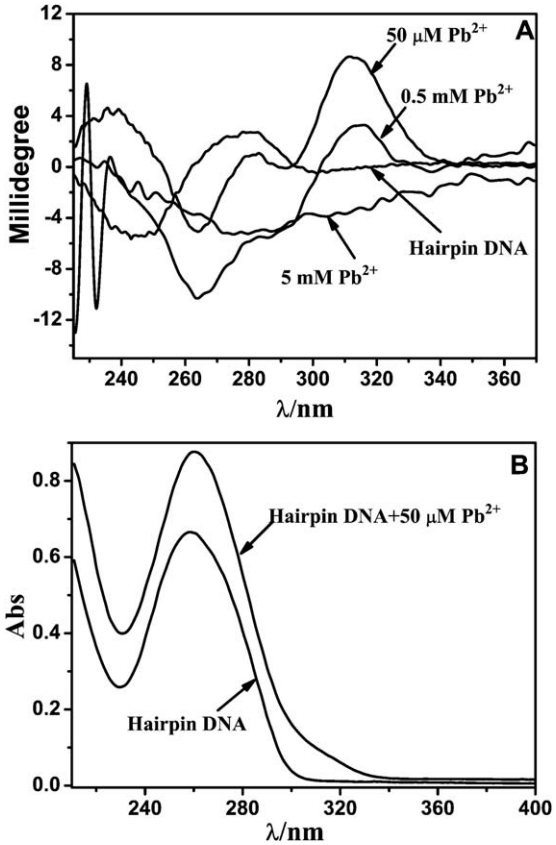


**Fig. 3** (A) CD spectra of 2 μM hairpin DNA(2) in the absence and in the presence of 5 mM, 0.5 mM and 50 μM $Pb^{2+}$; (B) UV-Vis spectra of 2 μM hairpin DNA(2) in the absence and in the presence of 50 μM $Pb^{2+}$.

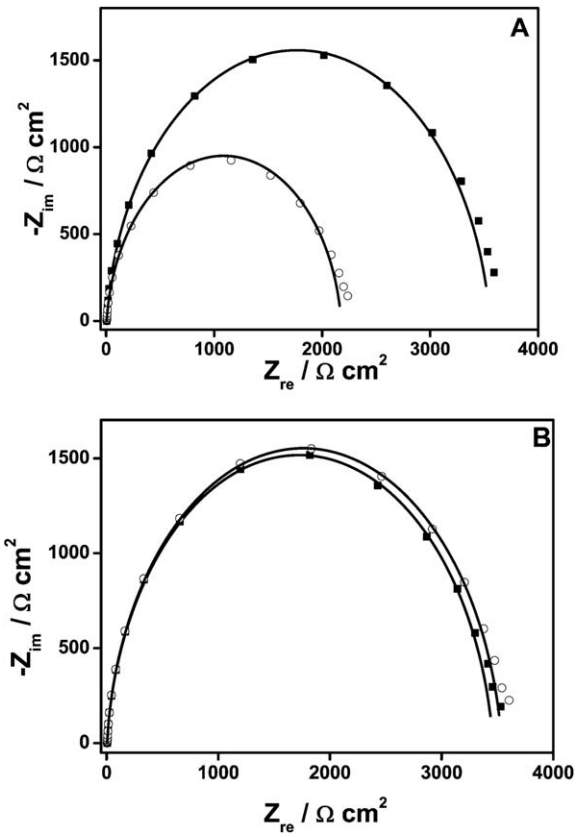


**Fig. 4** Representative Nyquist plots ($-Z_{im}$ *vs.* $Z_{re}$) for films of G-rich hairpin DNA(1) before (■) and after (○) incubating with (A) 5 mM $PbClO_4$ solution and (B) 0.5 mM $PbClO_4$ solution.

with 50 μM $Pb^{2+}$ (see the supporting information†). There was almost no change in the $R_{CT}$ observed. This indicated that the electrostatic interactions can be omitted when the concentration of $Pb^{2+}$ is not higher than 50 μM. In other words, the $R_{CT}$ increase in Fig. 2 is entirely caused by conformational swich.

In addition, it has been reported that $K^+$ can induce the G-rich DNA strand to form a G-quadruplex.[25–27,34] The impact of $K^+$ on the system was analyzed by CD and EIS, as shown in Fig. 5 The results demonstrated that there were almost no changes observed in both CD and EIS spectra. This was a strong proof that the interference of $K^+$ can be excluded. It should be noted that the interference of $Na^+$ was ignored in this assay because all used buffer solutions were 20 mM Tris-$NaClO_4$.

## 2 Theoretical computations

The structures of hairpin DNA, G-quadruplex and the G-quadruplex–$Pb^{2+}$ were optimized using DFT method (see the supporting information†). The G-quadruplex is 6.8 kcal $mol^{-1}$ higher than hairpin DNA in energy, implying that the hairpin structure is more stable than the G-quadruplex. The distance between two G4 planes is about 3.21 Å in the G-quadruplex structure. However, while the $Pb^{2+}$ was trapped between the two G4 planes, the distance decreased to 2.82 Å, and the average distance of the eight Pb–O distances is 2.58 Å, indicating that the interaction between $Pb^{2+}$ and G4 plane is rather strong. The formation of G-quadruplex–$Pb^{2+}$ is about 196 kcal $mol^{-1}$ exothermic. The exothermicity, which is too large, is probably a result of two factors: the first are the eight quite strong $Pb^{2+}\cdots O$ attractive interactions, and the hydrogen interactions in the G4 plane strengthened by the former interaction; the other is the solvent effect which is not considered. The solvent effect is expected to make the exothermic value smaller. All in all, the switch from hairpin to G-quadruplex–$Pb^{2+}$ is thermodynamically favorable and irreversible.

## 3 Sensitivity and selectivity

The detection limit of $Pb^{2+}$ based on this conformational switch by EIS was explored. Beginning with 50 μM, $\Delta R_{CT}$ is decreased with the decrease of $Pb^{2+}$ concentration as shown in Fig. 6A and Table 2. When the concentration of $Pb^{2+}$ is gradually reduced, only a part of hairpin DNA molecules can open the stem-loop structure to form the G-quadruplex, which leads to the decrease in $\Delta R_{CT}$ until the concentration of $Pb^{2+}$ decreased to 0.05 nM with no change in $R_{CT}$ observed.[31,33] Fig. 6A shows the relationship between $\Delta R_{CT}$ and concentration of $Pb^{2+}$ : $\Delta R_{CT}$ increases linearly with the logarithm of $Pb^{2+}$ concentration and the linear equation is $\Delta R_{CT} = -203.4 \times \log[Pb^{2+}]/\log[M] + 2294.6$ ($R = -0.999$). The result showed that $Pb^{2+}$ could be quantitatively measured over a large concentration variation from 50 μM to 0.5 nM and the detection limit is 0.5 nM, which is comparable and even lower than those of complicated

 

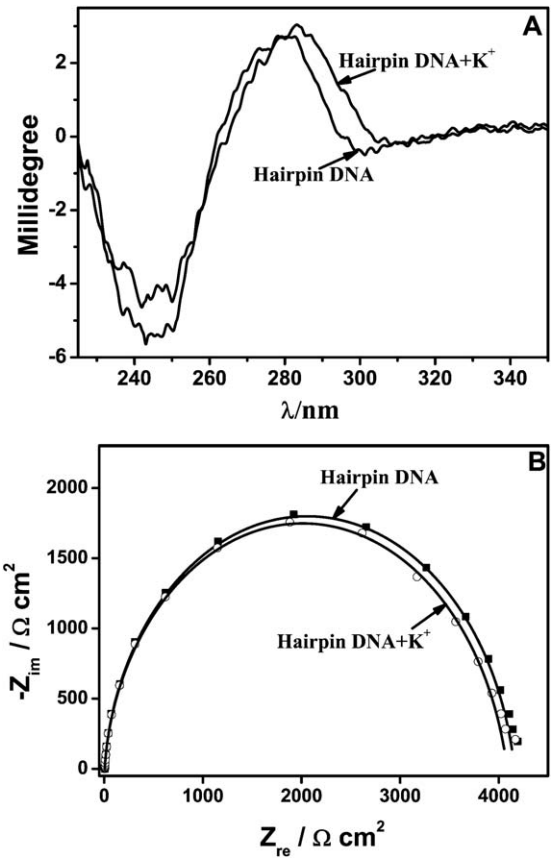


**Fig. 5** (A) CD spectra of 2 μM hairpin DNA(2) in the absence and presence of 50 mM $K^+$; (B) representative Nyquist plots ($-Z_{im}$ *vs.* $Z_{re}$) for films of hairpin DNA(1) before (■) and after (○) incubating with 5 mM $KClO_4$ solution after buffer washing.

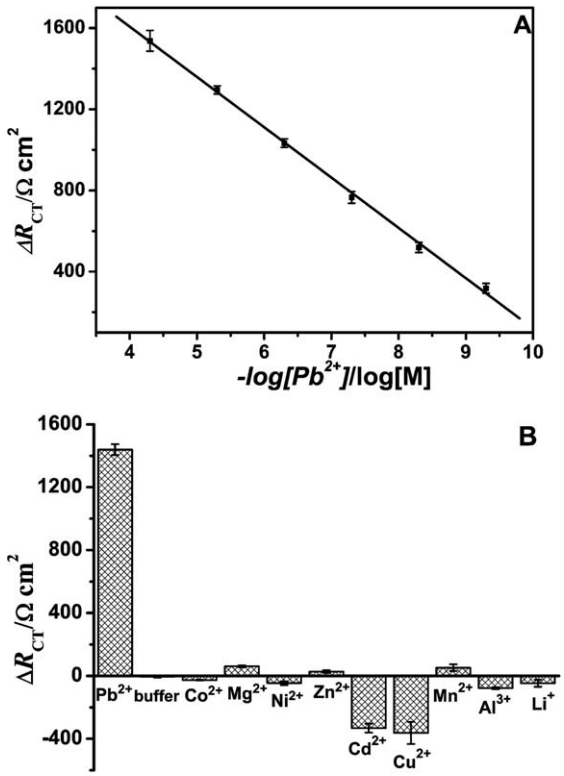


**Fig. 6** (A) Relationship between $\Delta R_{CT}$ and the concentration of $Pb^{2+}$. (B) Selectivity of hairpin DNA-based $Pb^{2+}$ sensor. The concentration of $Pb^{2+}$ and other metal ions (such as $Mg^{2+}$, $Zn^{2+}$, $Mn^{2+}$, $Co^{2+}$, $Ni^{2+}$, $Cd^{2+}$, $Cu^{2+}$, $Al^{3+}$, $Li^+$) were kept at $5 \times 10^{-5}$ M. Buffer: 20 mM Tris-$ClO_4$ (pH = 7.4). Error bars are derived from a minimum of five electrodes.

electrochemical, fluorescent, and colorimetric biosensors for $Pb^{2+}$ (see Supporting Information).

The selectivity of the assay was also explored. The values of $\Delta R_{CT}$ were analyzed upon adding other metal ions (such as $Co^{2+}$, $Mg^{2+}$, $Ni^{2+}$, $Zn^{2+}$, $Cd^{2+}$, $Cu^{2+}$, $Mn^{2+}$, $Al^{3+}$, $Li^+$) with the same concentration (50 μM) instead of $Pb^{2+}$ to the sensing system as shown in Fig. 6B. Only $Pb^{2+}$ caused a considerable large $\Delta R_{CT}$ while other ions yielded little ($Mg^{2+}$, $Zn^{2+}$, $Mn^{2+}$) or opposite ($Co^{2+}$, $Ni^{2+}$, $Cd^{2+}$, $Cu^{2+}$, $Al^{3+}$, $Li^+$) changes in $\Delta R_{CT}$, which indicated that response of the sensor to $Pb^{2+}$ was unaffected by the presence of the most possible contaminating ions. Therefore, this simple electrochemical sensor based on DNA conformational switch is highly selective for $Pb^{2+}$.

Finally, this assay was explored for detection $Pb^{2+}$ in newborn calf serum (see supporting information†). The results demonstrated that the complex medium did not interfere with the $Pb^{2+}$ detection.

## 4. Conclusion

In summary, we have investigated $Pb^{2+}$ induced DNA conformational switch from hairpin to G-quadruplex by electrochemical impedance spectroscopy (EIS), and an obvious

**Table 2** Equivalent circuit element values for hairpin DNA films in absence and presence of $Pb^{2+}$ [a]

| | Equivalent circuit elements | | | | | | |
|---|---|---|---|---|---|---|---|
| | $R_s/\Omega \cdot cm^2$ | $C_{monolayer}/\mu F \cdot cm^{-2}$ | $R_{CT}/\Omega \cdot cm^2$ | $R_x/\Omega \cdot cm^2$ | CPE/$\mu F \cdot cm^{-2}$ | $n$ | $\Delta R_{CT}/\Omega \cdot cm^2$ |
| Hairpin DNA(1) | 5.1(0.2) | 7.5(0.6) | 3340(146) | 4.0(0.6) | 11.3(1.3) | 0.8(0.01) | — |
| $5 \times 10^{-5}$ M | 5.2(0.5) | 9.7(0.2) | 4877(137) | 24.7(6.1) | 12.0(0.9) | 0.8(0.07) | 1537(51) |
| $5 \times 10^{-6}$ M | 5.1(0.2) | 10.1(1.3) | 4635(194) | 4.2(0.9) | 10.8(1.7) | 0.8(0.07) | 1295(20) |
| $5 \times 10^{-7}$ M | 5.3(0.4) | 8.6(0.3) | 4373(121) | 13.8(1.5) | 10.8(2.9) | 0.8(0.06) | 1033(21) |
| $5 \times 10^{-8}$ M | 5.3(0.2) | 9.0(0.1) | 4106(162) | 13.9(0.8) | 12.1(0.3) | 0.8(0.01) | 766(29) |
| $5 \times 10^{-9}$ M | 5.3(0.2) | 9.0(0.5) | 3859(274) | 17.8(8.1) | 7.8(3.2) | 0.8(0.01) | 519(25) |
| $5 \times 10^{-10}$ M | 5.3(0.2) | 8.3(0.6) | 3658(214) | 4.1(0.3) | 9.1(4.4) | 0.8(0.01) | 318(24) |

[a] The values in parentheses represent the standard deviations from at least 5 electrode measurements.

increased $R_{CT}$ was observed. DFT results indicated the switch from hairpin DNA to G-quadruplex induced by $Pb^{2+}$ is thermodynamically favorable and irreversible. Taking advantage of $R_{CT}$ differences, $\Delta R_{CT}$, $Pb^{2+}$ can be sensitively and selectively detected at a concentration as low as 0.5 nM. This assay was challenged by use of a complex medium, such as calf serum. Based on these results, a simple, low-cost and label-free electrochemical biosensor for $Pb^{2+}$ was constructed, which holds great potential for $Pb^{2+}$ in practical samples. In addition, the electrochemical approach based on the conformational switch can be further extended to other DNA-based systems to detect and quantify wider ranges of analytes.

This work is supported by grants from the Major State Basic Research Development Programs (Grant No. 2009CB421605 and 2011CB808503) and the NSFC (Grant No. 21073019).

## References


1 Q. W. He, E. W. Miller, A. P. Wong and C. Chang, *J. Am. Chem. Soc.*, 2006, **128**, 9316–9317.
2 H. Wang, Y. Kim, H. P. Liu, Z. Zhu, S. Bamrungsap and W. H. Tan, *J. Am. Chem. Soc.*, 2009, **131**, 8221–8226.
3 D. P. Wernette, C. Mead, P. W. Bohn and Y. Lu, *Langmuir*, 2007, **23**, 9513–9521.
4 J. Li and Y. Lu, *J. Am. Chem. Soc.*, 2000, **122**, 10466–10467.
5 J. W. Liu, A. K. Brown, X. L. Meng, D. M. Cropek, J. D. Istok, D. B. Watson and Y. Lu, *Proc. Natl. Acad. Sci. U. S. A.*, 2007, **104**, 2056–2061.
6 T. Lan, K. Furuya and Y. Lu, *Chem. Commun.*, 2010, **46**, 3896–3898.
7 J. Liu and Y. Lu, *Anal. Chem.*, 2003, **75**, 6666–6672.
8 C. B. Swearingen, D. P. Wernette, D. M. Cropek, Y. Lu, J. V. Sweedler and P. W. Bohn, *Anal. Chem.*, 2005, **77**, 442–448.
9 X. B. Zhang, Z. D. Wang, H. Xing, Y. Xiang and Y. Lu, *Anal. Chem.*, 2010, **82**, 5005–5011.
10 T. S. Dalavoy, D. P. Wernette, M. Gong, J. V. Sweedler, Y. Lu, B. R. Flachsbart, M. A. Shannon, P. W. Bohn and D. M. Cropek, *Lab Chip*, 2008, **8**, 786–793.
11 J. W. Liu and Y. Lu, *J. Am. Chem. Soc.*, 2003, **125**, 6642–6643.
12 J. W. Liu and Y. Lu, *J. Am. Chem. Soc.*, 2004, **126**, 12298–12305.
13 J. W. Liu and Y. Lu, *J. Am. Chem. Soc.*, 2005, **127**, 12677–12683.
14 Z. D. Wang, J. H. Lee and Y. Lu, *Adv. Mater.*, 2008, **20**, 3263–3267.
15 D. Mazumdar, J. W. Liu, G. Lu, J. Z. Zhou and Y. Lu, *Chem. Commun.*, 2010, **46**, 1416–1418.
16 J. Elbaz, B. Shlyahovsky and I. Willner, *Chem. Commun.*, 2008, 1569–1571.
17 T. Li, E. K. Wang and S. J. Dong, *Anal. Chem.*, 2010, **82**, 1515–1520.
18 C. W. Liu, C. C. Huang and H. T. Chang, *Anal. Chem.*, 2009, **81**, 2383–2387.
19 X. Zhu, Z. Y. Lin, L. F. Chen, B. Qiu and G. N. Chen, *Chem. Commun.*, 2009, 6050–6052.
20 Y. Xiang, A. Tong and Y. Lu, *J. Am. Chem. Soc.*, 2009, **131**, 15352–15357.
21 Y. Xiang, Z. D. Wang, H. Xing, N. Y. Wong and Y. Lu, *Anal. Chem.*, 2010, **82**, 4122–4129.
22 Y. Xiao, A. A. Rowe and K. W. Plaxco, *J. Am. Chem. Soc.*, 2007, **129**, 262–263.
23 L. Shen, Z. Chen, Y. H. Li, S. L. He, S. B. Xie, X. D. Xu, Z. W. Liang, X. Meng, Q. Li, Z. W. Zhu, M. X. Li, X. C. Le and Y. H. Shao, *Anal. Chem.*, 2008, **80**, 6323–6328.
24 X. R. Yang, J. Xu, X. M. Tang, H. X. Liu and D. B. Tian, *Chem. Commun.*, 2010, **46**, 3107–3109.
25 I. Smirnov and R. H. Shafer, *J. Mol. Biol.*, 2000, **296**, 1–5.
26 I. V. Smirnov, F. W. Kotch, I. J. Pickering, J. T. Davis and R. H. Shafer, *Biochemistry*, 2002, **41**, 12133–12139.
27 P. R. Majhi and R. H. Shafer, *Biopolymers*, 2006, **82**, 558–569.
28 T. Yanai, D. P. Tew and N. C. Handy, *Chem. Phys. Lett.*, 2004, **393**, 51–57.
29 M. J. Frisch, G. W. Trucks, H. B. Schlegel, *Gaussian 09, Revision A.02*; Gaussian, Inc, Wallingford CT, 2009.
30 D. M. Jenkins, B. Chani, M. Kreuzer, G. Presting, A. M. Alvarez and B. Y. Liaw, *Anal. Chem.*, 2006, **78**, 2314–2318.
31 A. E. Radi and C. K. O'Sullivan, *Chem. Commun.*, 2006, 3432–3434.
32 M. Dijksma, B. A. Boukamp, B. Kamp and W. P. van Bennekom, *Langmuir*, 2002, **18**, 3105–3112.
33 H. Gong, T. Y. Zhong, L. Gao, X. H. Li, L. J. Bi and H. B. Kraatz, *Anal. Chem.*, 2009, **81**, 8639–8643.
34 M. Vairamani and M. L. Gross, *J. Am. Chem. Soc.*, 2003, **125**, 42–43.